Journal of GeoEngineering, Vol. 19, No. 1, pp. 001-016, March 2024
http://dx.doi.org/10.6310/jog.202403_19(1).1

NUMERICAL INVESTIGATION OF RESPONSE MECHANISMS OF A SINGLE PILE UNDER GROUND DEFORMATION AND RUPTURE INDUCED BY REVERSE FAULTING

Jiunn-Shyang Chiou [1*], Yi-Wun Lee [2], and Cheng-En Ho [3]

ABSTRACT

Fault dislocation can cause ground deformation and even rupture, thereby directly influencing the behavior of structure foundations. The mechanisms underlying the response of a foundation are complex. This study performs three-dimensional finite element analyses to investigate the mechanisms underlying single-pile responses under the actions of ground deformation and rupture due to reverse faulting. In the analyses, we assume that a single pile is embedded in cohesionless soil and that reverse faulting occurs. A centrifuge test reported in the literature is simulated to validate the numerical model and calibrate the model's parameters. In the parametric analyses, we consider pile location with respect to the initial location of the fault tip. The results reveal that the pile response depends on the degree of fault offset and relative distance between the pile and fault tip. Different positions of the main ground deformation or rupture zone with respect to the pile exhibit different pile response mechanisms. With increasing fault offset, three and two response mechanisms are identified for the conditions before and after the ground rupture reaches the pile, respectively.

Key words: Fault dislocation, reverse faulting, centrifuge tests, ground rupture, finite element analysis.

1. INTRODUCTION

Engineering structures are not normally built on or near the traces of active faults. However, this is nearly impossible to achieve it in areas with a high density of fault lines. Structures situated on or near active faults may suffer damage when a fault ruptures. In many historic earthquakes, fault rupture caused severe damage to infrastructure, such as bridges, buildings, and utilities (Chen *et al.* 2003; Anastasopoulos and Gazetas 2007; Anastasopoulos *et al.* 2008; Faccioli *et al.* 2008; Yang *et al.* 2018). When a fault dislocates, the ground above it deforms and ruptures further with increasing fault offset. Even if structures are not located immediately on the fault, they may be influenced by this induced ground movement; for example, pipelines can break and structure foundations can suffer displacement or damage (Oettle and Bray 2013; Rasouli and Fatahi 2019; Fadaee *et al.* 2020).

Structure foundations are directly affected by fault ruptures, and their displacement or damage influences the serviceability and safety of structures. Numerous experimental and numerical studies have been conducted on the influence of ground rupture on foundation behavior (Anastasopoulos *et al.* 2008a, 2008b; Bransby *et al.* 2008; Cai and Ng 2016; Li *et al.* 2019; Naeij *et al.* 2019; Yao and Takemura 2020). Bransby *et al.* (2008) conducted centrifuge testing on shallow foudations subjected to reverse faulting and discovered that the response of the foundations was influenced by their rigiditiy and structure loads, which could also change the path of ground ruputure. Anastasopoulos *et al.* (2008a) conducted finite element analyses to simulate the responses of group-pile and caisson foundations subjected to ground rupture of normal faults. They found that these two types of foundations responded differently to ground rupture and that the foundation-fault tip distance and soil stiffness were the main factors influencing the foundation's response. Cai and Ng (2016) performed centrifuge testing on a single pile and a group of three piles subjected to normal faulting. They found that the single pile was displaced and the pile top was rotated toward the hanging wall; the middle pile of the group, which was in the hanging wall, failed in tension and was subjected to negative skin friction owing to the relative downward displacement of the soil around the pile. Li *et al.* (2019) conducted model tests and numerical analyses to simulate the behavior of group-pile foundations subjected to reverse faulting. The pile cap subjected to fault-induced ground movement underwent lateral displacement and rotation, and the pile's response differed at different positions. Naeij *et al.* (2019) conducted numerical analyses to simulate the behavior of embedded shallow foundations subjected to reverse faulting. They revealed that the path of ground rupture propagation was affected by the foundation embedment. Yao and Takemura (2020) performed centrifuge testing on single piles under dip-slip faulting and found that the piles sustained larger bending moments and axial loads under reverse faulting than under normal faulting.

These studies concluded that different foundation types exhibit differing responses to fault rupture and differing influences on the development of ground rupture. Most studies have focused on the fault-induced macro responses of foundations; however, the interaction of foundations with ground movement remains unclear. Therefore, the present study investigates the detailed mechanisms of pile-soil interaction for single-pile foundations under reverse

Manuscript received May 18, 2023; revised November 18, 2023; accepted January 16, 2024.
[1*] Associate Professor (corresponding author), Department of Civil Engineering, National Taiwan University, Taipei, Taiwan (e-mail: jschiou@ntu.edu.tw).
[2] Former Master Student, Department of Civil Engineering, National Taiwan University, Taipei, Taiwan.
[3] Ph.D. Student, Department of Civil Engineering, National Taiwan University, Taipei, Taiwan.

faulting by conducting three-dimensional finite element analysis. The soil model used is the porous elasticity model combined with the Drucker-Prager/Cap plasticity model. The numerical model is validated by simulating a centrifuge test reported in the literature (Yao and Takemura 2020). To comprehensively investigate the complex pile-soil interaction, parametric analyses are conducted in which various positions relative to the fault tip are considered. By observing the responses of the pile and soil as well as those of the free-field ground, the mechanisms of pile-soil interaction due to reverse faulting are clearly identified in terms of the position of the main ground deformation or rupture zone acting on the pile.

2. DEVELOPMENT AND VALIDATION OF ANALYSIS MODEL

2.1 Model Description

The finite element model is constructed using ABAQUS (ABAQUS 2012) and employed to analyze the response of single piles subjected to reverse faulting. The model has three main parts: the pile, soil, and pile-soil interface. The pile is simulated using C3D8 solid elements (3D eight-noded elements) and is assumed to be elastic. The soil is also simulated by C3D8 elements and is assumed to be elastoplastic. Slippage and separation between the soil and pile are allowed. The surface-to-surface contact mode is adopted to simulate the contact behavior of the pile-soil interface, in which the pile and soil surfaces are set as master and slave surfaces, respectively. The normal behavior of the pile-soil interface is assumed to be hard contact (the normal stress only exists when the soil and pile are in contact). The Coulomb friction model is adopted to simulate the tangential shear behavior of the pile-soil interface. Given the materials constituting the pile and soil, the coefficient of friction of the pile-soil interface conforms with the values stipulated in NAVFAC DM-7.2 (1982).

2.2 Soil Model

In the present study, cohesionless soil is considered. For simulating the behavior of cohesionless soil, the porous elasticity model and Drucker-Prager/Cap model are used to describe the elastic and plastic behaviors of the soil, respectively. These two models are briefly described as follows (ABAQUS 2012).

1. Porous elasticity model

This model assumes that the increment in elastic volumetric strain is proportional to the logarithmic compressive stress, as illustrated in Fig. 1(a); this relationship is expressed as follows:

$$\frac{\kappa}{1+e_0}\ln\left(\frac{p_0+p_t^{el}}{p+p_t^{el}}\right)=\varepsilon_{ve} \tag{1}$$

where e_0 is the initial void ratio, p is the mean stress, p_t^{el} is the tensile strength under the elastic state, p_0 is the initial confining pressure, ε_{ve} is the elastic volumetric strain, and κ is the logarithmic bulk modulus.

2. Drucker-Prager/Cap model

In this model, a yield surface comprising two parts is defined as displayed in Fig. 1(b).

The first part is the linear shear failure surface:

$$F_s=t-p\tan\beta-d=0 \tag{2}$$

where t is the deviatoric stress, p is the equivalent confining stress, and β and d are the slope and intercept of the surface on the t-p plane, respectively.

Here, t and p are respectively defined as

$$t=\frac{1}{2}q\left[1+\frac{1}{K}-\left(1-\frac{1}{K}\right)\left(\frac{r}{q}\right)^3\right] \tag{3}$$

$$p=\frac{\sigma_1+\sigma_2+\sigma_3}{3} \tag{4}$$

where σ_1, σ_2, and σ_3 are the maximum, intermediate, and minimum principal stresses, respectively; q is the Mises equivalent stress $\left(q=\sqrt{3/2(S_{ij}\,S_{ij})}\right)$, in which S_{ij} is the deviatoric stress tensor); r is the third invariant of the deviatoric stress $\left(r=\left(\frac{9}{2}S_{ij}\,S_{jk}\,S_{ki}\right)^{1/3}\right)$; and K is the yield stress ratio of triaxial tension to triaxial compression.

The parameters β, d, and K can be determined on the basis of the parameters of the Mohr-Coulomb model by using the following equations:

$$\tan\beta=\frac{6\sin\phi}{3-\sin\phi} \tag{5}$$

$$d=2c\frac{\cos\phi}{1-\sin\phi}\left(1-\frac{\tan\beta}{3}\right) \tag{6}$$

$$K=\frac{3-\sin\phi}{3+\sin\phi} \tag{7}$$

where c is the cohesion and ϕ is the friction angle associated with the Mohr-Coulomb model. For a yield surface to be concave, K must be between 0.778 and 1 (ABAQUS 2012).

The second part is the compressive cap yield surface; it is a movable surface, the position of which depends on the hydrostatic compression yield stress p_b, and it is defined as follows:

$$F_c=\sqrt{(p-p_a)^2+(Rt)^2}-R(d+p_a\tan\beta)=0 \tag{8}$$

where R is the cap eccentricity and $p_a=\frac{p_b-Rd}{1+R\tan\beta}$.

To describe the hardening behavior of the cap yield surface, a volumetric strain hardening curve is defined for the relationship between p_b and the plastic volumetric strain ε_{vp}, as illustrated in Fig. 1(c).

2.3 Verification of Analysis Model

Yao and Takemura (2020) conducted a series of centrifuge tests on single piles under dip-slip faulting. To demonstrate the applicability of the 3D finite element analysis model constructed in the present study, one of their tests is simulated. The selected test is a single pile subjected to reverse faulting with a 60° dip. A centrifugal gravity of 50 g was adopted in the test. Regarding the prototype, the pile was a square pile of size 0.5 m with an embedded length of 10 m; the pile was embedded in Toyoura sand having a relative density of approximately 80%.

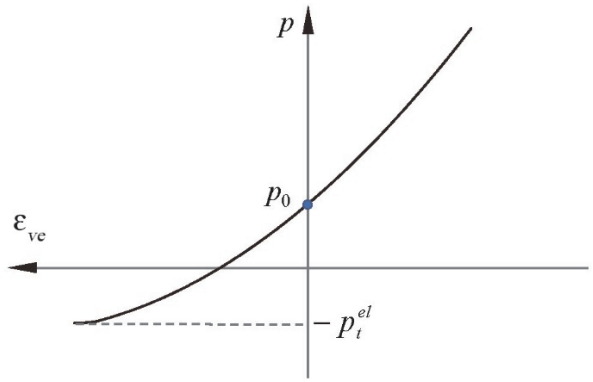

(a) Porous elasticity model

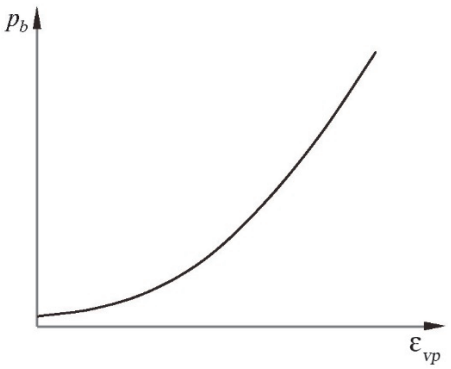

(c) Strain-hardening curve for the cap model

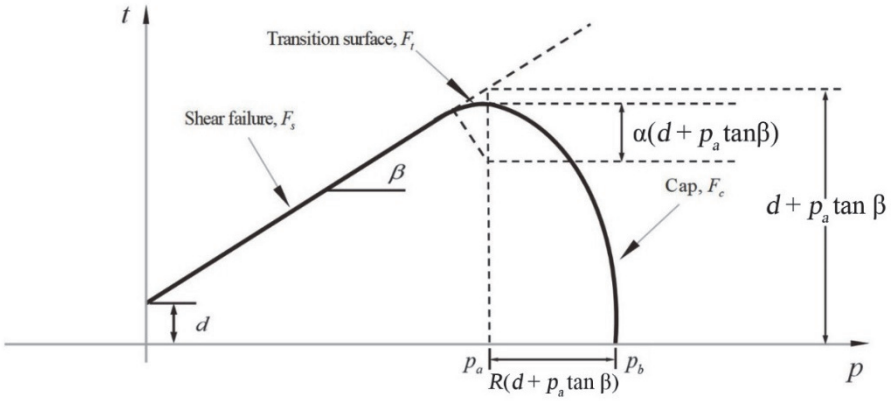

(b) Drucker-Prager/Cap model

Fig. 1 Soil model (ABAQUS 2012)

To calibrate the parameters of the soil model, the drained triaxial compression tests on Toyoura sand conducted by Fukushima and Tatsuoka (1984) under a similar density condition to that in the centrifuge test are simulated. Figure 2 presents the comparison of the numerical and experimental deviatoric stress-axial strain curves for different confining pressures of 49, 98, and 196 kPa; the overall soil behavior, including the strain-softening response, is reasonably captured. Tables 1 and 2 present the calibrated parameters for the porous elasticity model and Drucker-Prager/Cap model, respectively, and Fig. 3 shows the hardening curve. Notably, considering the actual nonlinear peak-strength envelope of the soil, the angle of friction β is varied with the corresponding effective confining pressure; the angles of friction under effective confining pressures of 49, 98, and 196 kPa are set as 60.5°, 59°, and 59°, respectively.

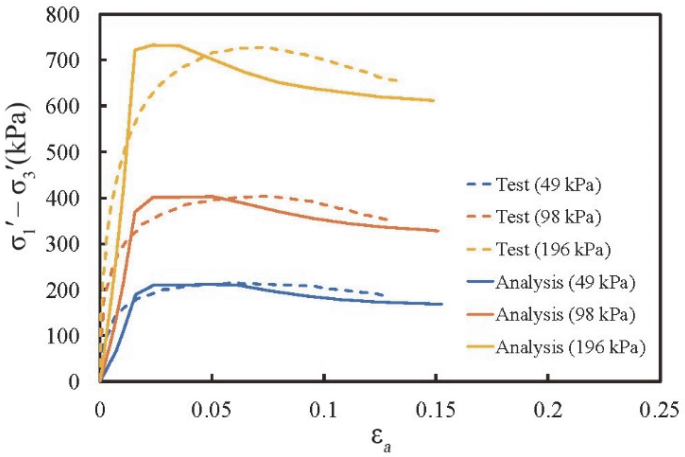

Fig. 2 The comparison of numerical and experimental deviatoric stress-axial strain curves under confining pressures of 49, 98, and 196 kPa (Test data are from Fukushima and Tatsuoka 1984)

The model tests mentioned previously for the free-field ground condition and ground with a single pile are simulated. Because of complicated soil conditions of the centrifuge tests, which may not be completely the same as in the soil element tests, for a better simulation of ground and pile responses, the soil parameters of κ and the initial yield surface position in Tables 1 and 2 are slightly modified to vary with depth, as presented Table 3. Figure 4(a) presents the finite element model for the free-field

Table 1 Parameters for porous elasticity model

Log bulk modulus, κ	Poisson's ratio, ν	Tensile limit, p_t^{el}
0.012	0.3	0

Table 2 Parameters for Drucker–Prager/Cap model

Material cohesion, d (kPa)	Friction angle, β (°)	Cap eccentricity, R	Initial yield surface position	Transition surface radius, α	Flow stress ratio, K
0.01	59-60.5	0.5	0.2	0.1	0.778

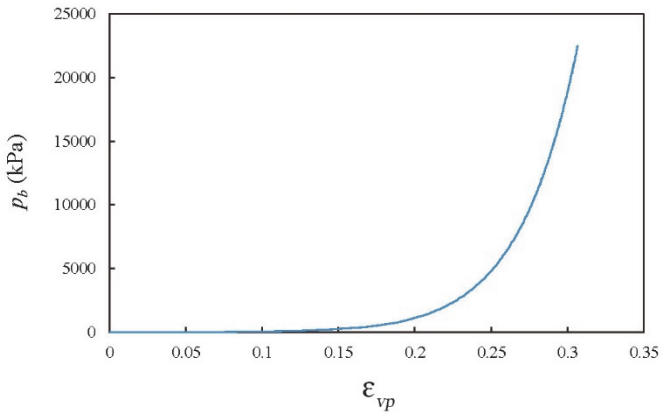

Fig. 3 Strain hardening curve

Table 3 Modified κ and the initial yield surface position in the simulation of the centrifuge tests

Depth (m)	Log bulk modulus κ	Initial yield surface position
0-1	0.025	0.2
1-2	0.025	0.2
2-3	0.02	0.2
3-4	0.02	0.2
4-5	0.012	0.2
5-6	0.012	0.2
6-7	0.012	0.2
7-8	0.012	0.2
8-9	0.012	0.19
9-10	0.012	0.18
10-11	0.012	0.18

ground condition. The initial fault tip location is a distance of 7.35 m from the left edge of the model. According to previous studies regarding foundation-soil interaction problems (Chiou and You 2020; Chiou and Wei 2021), an element size of 1/20-1/10 foundation length for the soil is generally set, considering the numerical precision and computational capacity. Thus, in the present study, an element size of 0.5 m is set for the soil element. This element size is also finer that 1 m, which is commonly used in research for fault rupture problems (Anastasopoulos *et al.* 2007).

The finite element model for the ground with a single pile is shown in Fig. 4(b). In this case, the pile is set 3.75 m from the right-hand side of the fault tip. The pile's length is 11 m, and 10 m of this is embedded in the ground. The flexural rigidity of the pile is 1.64×10^4 kN-m^2, with the element size being 0.125 m. Considering the diameter of pile, this pile element size is finer than soil element size for obtaining the axial force variation to compute the bending moments of the pile. The upward vertical offset (δ_V) and rightward horizontal offset (δ_H) are set to the model boundary at the left-hand side of the fault tip to simulate reverse faulting with a 60° dip and to freely generate ruptures in the ground.

Figure 5 presents comparisons of the numerical and experimental ground ruptures and ground-surface vertical displacements of the model test at vertical fault offset δ_V to ground thickness H ratios of 3.94% and 11.8% under the free-field condition. There were two ground rupture lines RF1 and RF2 observed in the test, in which RF1 occurred earlier than RF2 (Yao and Takemura 2019). The numerical rupture progress is similar to the experimental one, as indicated in Figs. 5(a) and 5(b). As RF1 and RF2 observed in the test, the numerical results present that there are also two ruptures (one occurs first), and with an increasing fault offset, the ground rupture moves upward and leftward. In addition, the numerical ground-surface vertical displacement profiles at offsets δ_V/H = 3.94% and 11.8% are similar to the experiment ones, as indicated in Fig. 5(c).

Figure 6 presents the simulation results for the model test under a vertical fault offset δ_V to ground thickness H ratio of 11.8%. Under the free-field condition, the ground ruptures, as indicated in Fig. 6(a). The solid blue line in Fig. 6(c) is the simulated ground horizontal displacement profile at a distance of 3.75 m from the initial fault tip (which is the prescribed pile location). At a depth approximately 6-8 m, an abrupt displacement change occurs to form a plateau. This displacement profile is unique to ground under reverse faulting. Above the plateau, the ground has a large displacement (hanging wall); below the plateau, the ground displacement is much smaller (footwall). Further, the simulated displacement profile is in agreement with the experimental profile (dashed blue line).

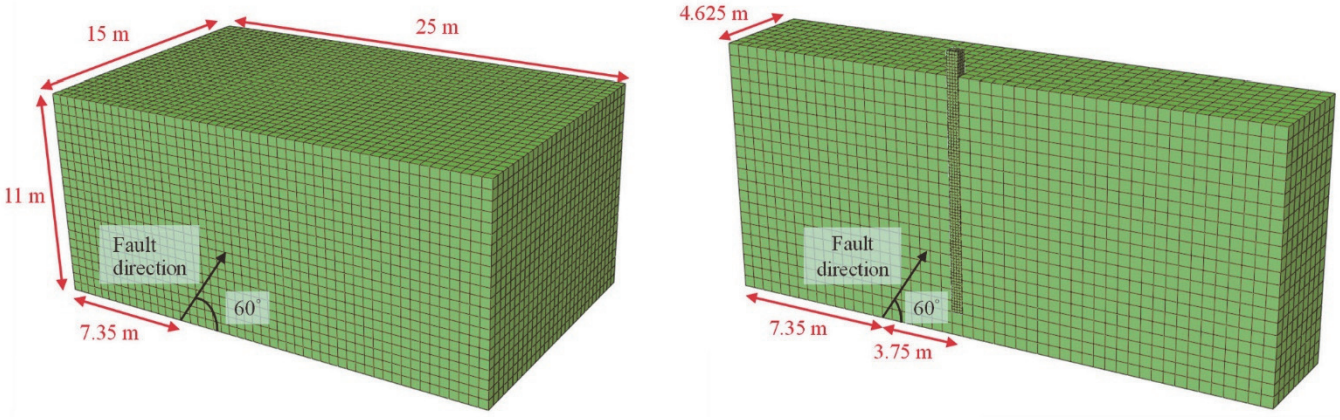

(a) Free-field condition (b) Ground with a single pile

Fig. 4 Numerical models of the model tests under reverse faulting

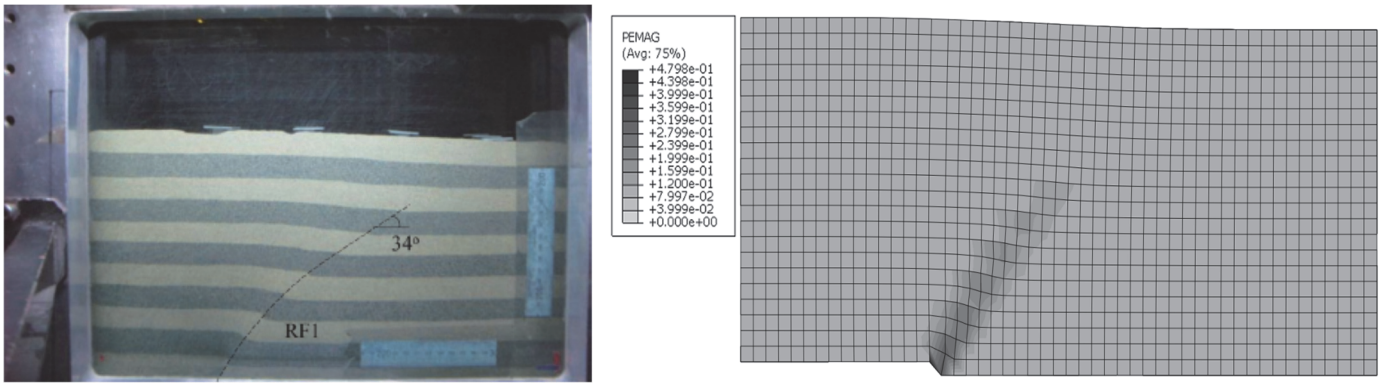

(a) Ground rupture (δ_V/H = 3.94%)

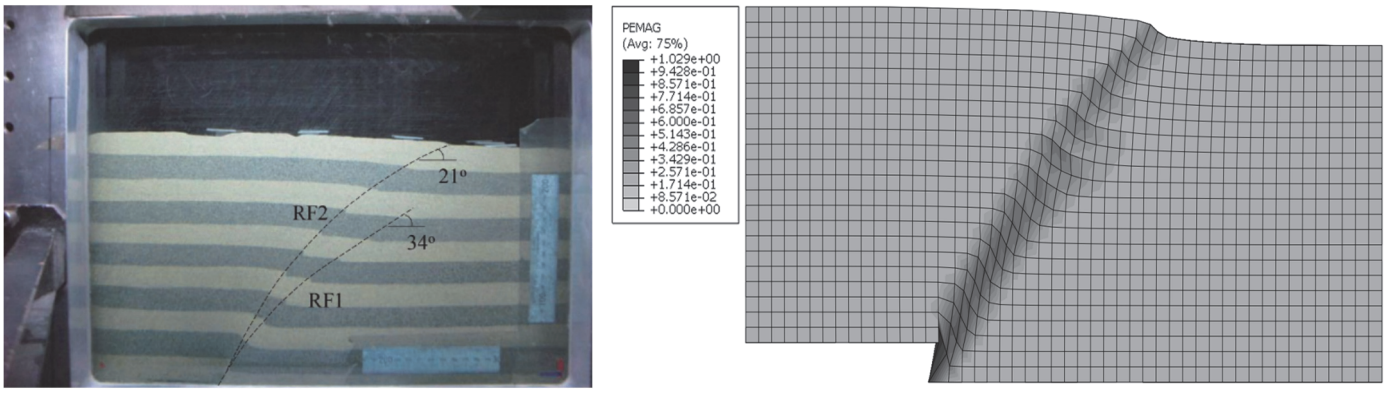

(b) Ground rupture (δ_V/H = 11.8%)

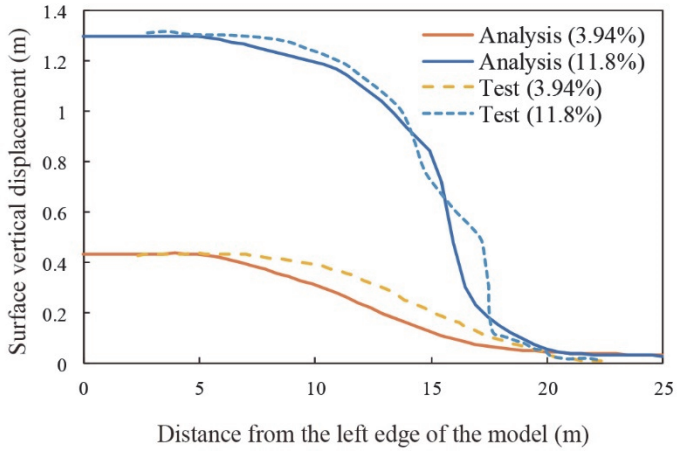

(c) Ground-surface vertical displacement

Fig. 5 Comparisons of numerical and experimental ground ruptures and ground-surface vertical displacement profiles at offsets δ_V/H = 3.94% and 11.8% under the free field condition (Test data are from Yao and Takemura 2019)

For a single pile in the ground subjected to the same fault offset (δ_V/H = 11.8%), a comparison of Figs. 6(a) and 6(b) shows that the lower portion of the pile is in the footwall of the rupture; because of the existence of the pile, the development of the ground rupture is changed. Figs. 6(c) to 6(f) presents comparisons of the numerical and experimental ground horizontal displacement, pile horizontal displacement, moment, and axial force profiles with depth, respectively. For the ground horizontal displacement profiles (orange lines in Fig. 6(c)), the numerical and experimental displacements are close near the pile head, and a slight underestimation is seen at depths below 2 m; they are similar to those in the free-field condition. For the pile horizontal displacement profiles (Fig. 6(d)), the pile displacement is found to be underestimated; the overall trends are similar. For the moment profiles (Fig. 6(e), positive value represents the right-half side of the pile cross section sustains tension), the moment is discovered to be underestimated, and the maximum moment occurs at a depth of about 5 m. Regarding the axial force profiles (Fig. 6(f), positive value implies tension), the axial force is overestimated around the middle part of the pile, including the location of the maximum axial force. Despite these deviations, the aforementioned analyses reveal that our finite element analysis model can reasonably simulate ground rupture and its impacts on the response of a pile under reverse faulting.

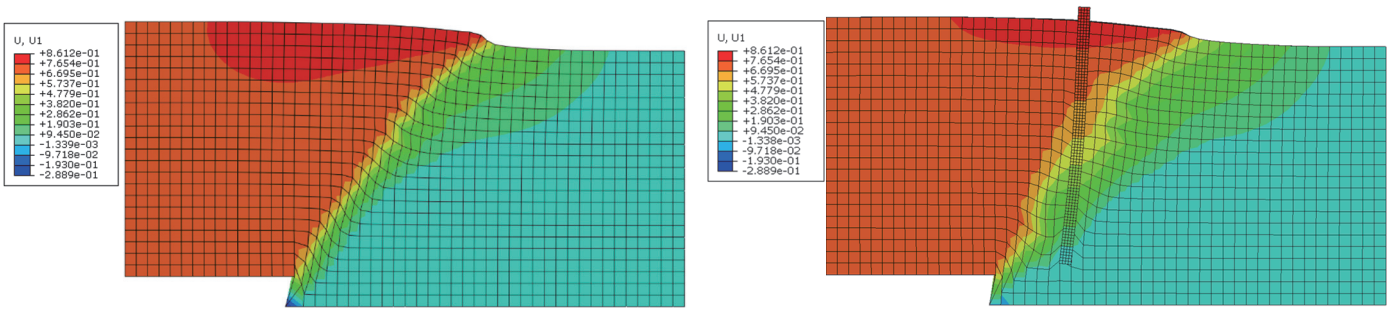

(a) Displacement field (free-field)

(b) Displacement field (with pile)

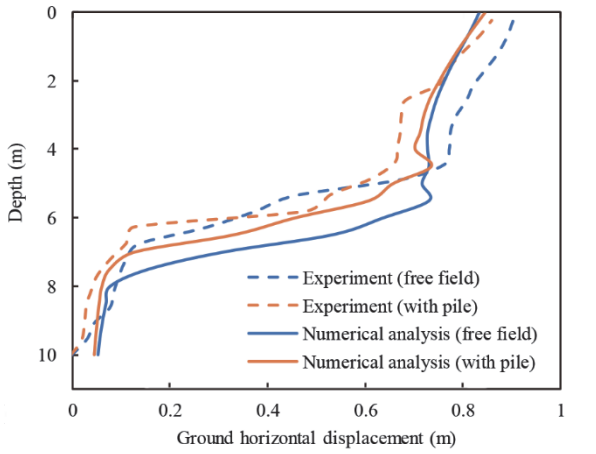

(c) Simulated and measured ground horizontal displacement profiles

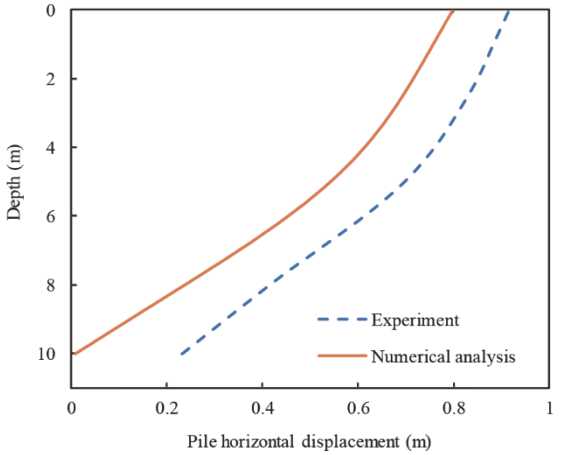

(d) Simulated and measured pile horizontal displacement profiles

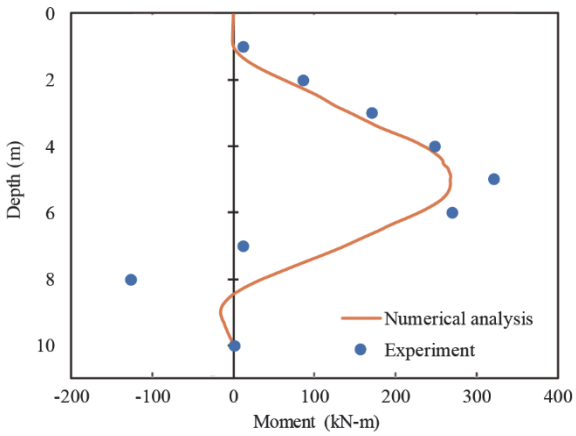

(e) Simulated and measured moment profiles

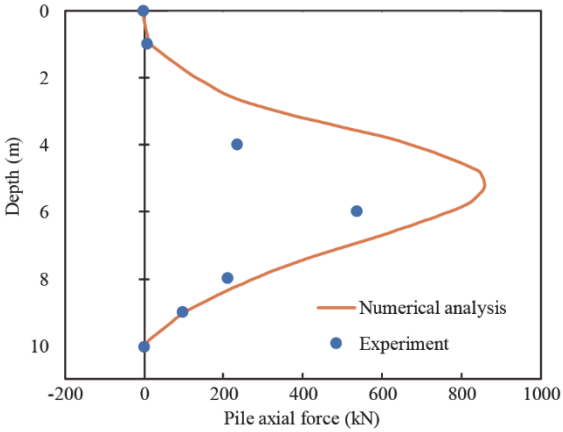

(f) Simulated and measured axial force profiles

Fig. 6 Simulation results of the model test at an offset δ_V/H = 11.8%

3. PARAMETRIC ANALYSIS

With the proposed numerical model and soil parameters in Tables 1 and 2, a series of finite element analyses is performed to investigate the ground deformation patterns due to reverse faulting and their influences on the pile-soil interaction.

3.1 Free-Field Ground Responses Due to Reverse Faulting

A 3D finite element analysis for the free-field ground condition is performed. Figure 7 presents a schematic of the analysis model. The model is a ground model with length, width, and thickness of 85, 60, and 30 m, respectively; it is subjected to reverse faulting with a dip 60°. The initial fault tip is set from 15 m relative to the left side of the model. The vertical displacement δ_V

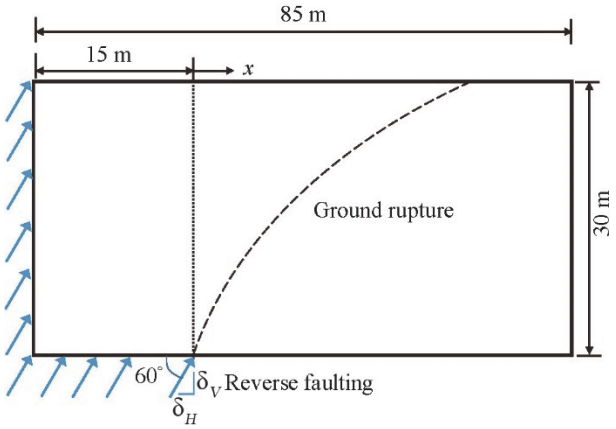

Fig. 7 Schematic diagram of the analysis model

and horizontal displacements δ_H are controlled to simulate a particular fault offset along the prescribed dip direction. The maximum vertical offset component is δ_V/H = 10%. The characteristics of the displacement responses due to reverse faulting are discussed in the following.

Figure 8 shows the ground displacement and soil plastic shear strain fields under reverse faulting at a fault offset of δ_V/H = 10%. The plastic shear strain zone is fully developed to the ground surface; this causes a pronounced offset at the surface, with this offset being located at approximately 21 m from the fault tip. The ground displacement of the hanging wall is much larger than that of the footwall because of plastic shear deformation along the rupture band.

Figure 9 presents the horizontal and vertical displacements with the fault offset at a varying distance x from the fault tip. The

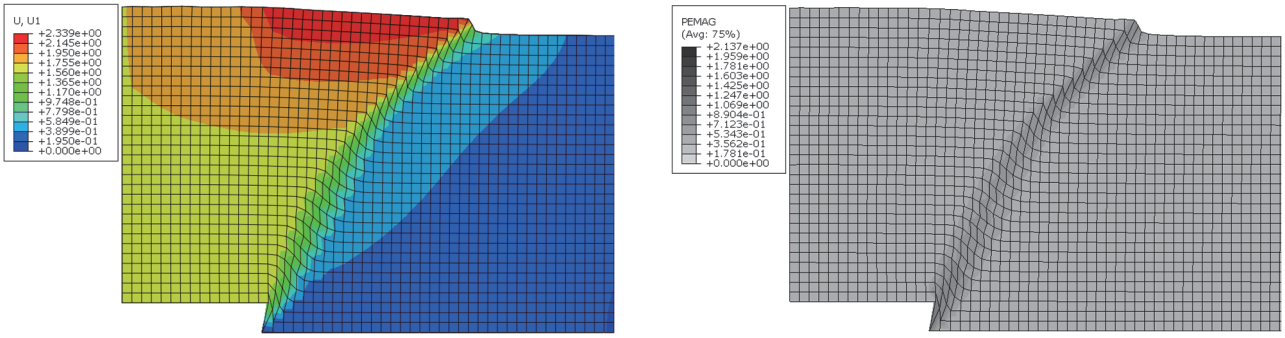

(a) Horizontal ground displacement (b) Plastic shear strain

Fig. 8 Horizontal ground displacement and plastic shear strain fields subjected to reverse faulting at a fault offset of δ_V/H = 10%

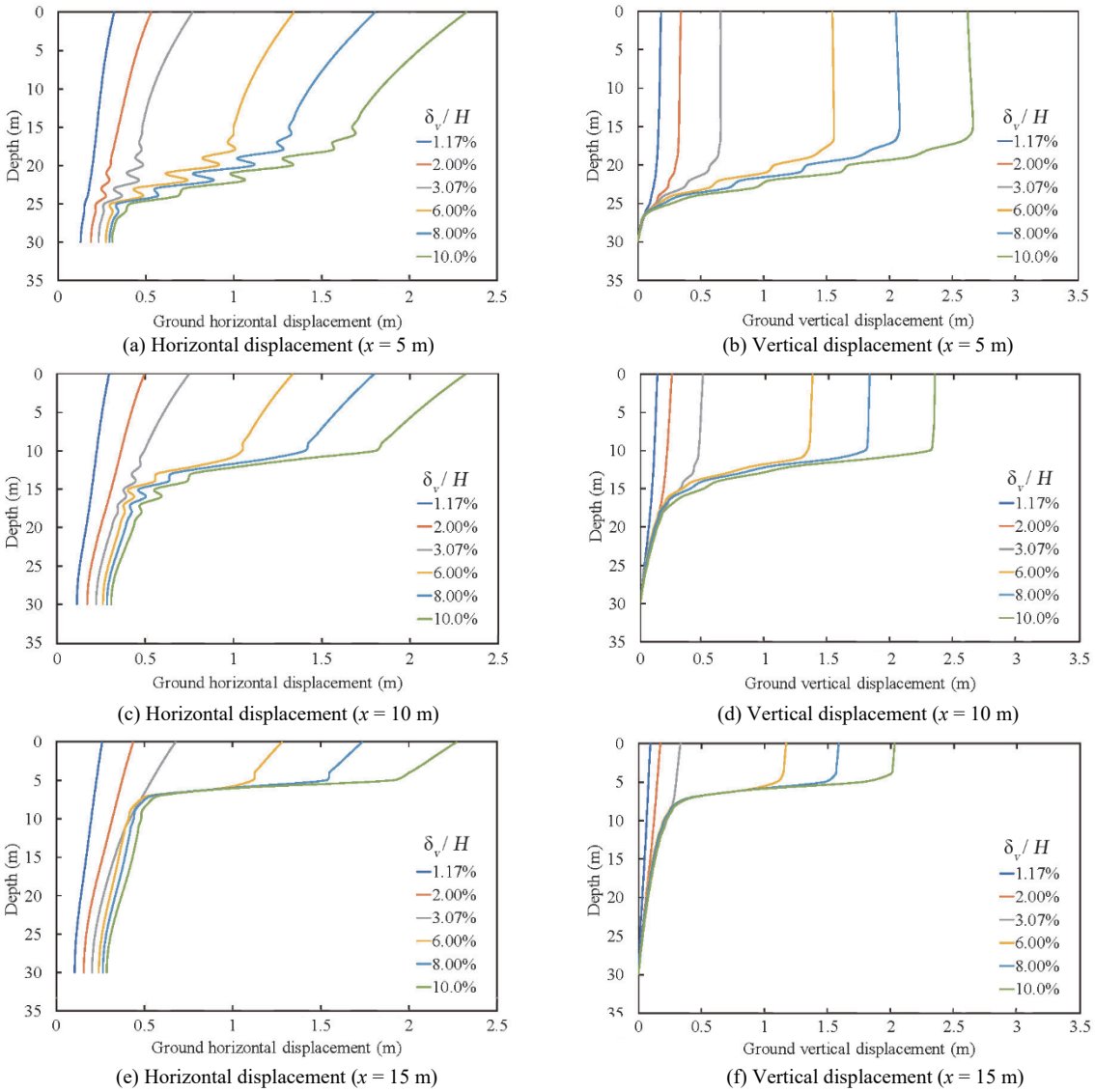

(a) Horizontal displacement (x = 5 m) (b) Vertical displacement (x = 5 m)

(c) Horizontal displacement (x = 10 m) (d) Vertical displacement (x = 10 m)

(e) Horizontal displacement (x = 15 m) (f) Vertical displacement (x = 15 m)

Fig. 9 Displacement evolution under reverse faulting

displacements within the main rupture zones present pronounced fluctuation, which indicates large distortions around these areas due to shearing. For x = 5 m, as illustrated in Figs. 9(a) and 9(b), the ground displacement increases with increasing fault offset. At δ_V/H of approximately 2%, a clear discontinuity (abrupt displacement change) occurs at a depth of approximately 18-25 m; for a larger offset, the discontinuity is more evident. This observation indicates that the depth range of 18-25 m is a rupture zone; a depth smaller than this is considered the hanging wall, and a depth larger than this is considered the footwall. Similarly, for x = 10 m, as presented in Figs. 9(c) and 9(d), at δ_V/H of approximately 3.07%, a rupture zone is evident at a depth of approximately 11-16 m. For x = 15 m (Figs. 9(e) and 9(f)) and at δ_V/H of approximately 6%, a rupture zone is formed at a depth of approximately 5-8 m. These observations reveal that the larger the distance to the fault tip, the larger is the offset required to generate the ground rupture and the shallower is the rupture zone.

3.2 Pile Responses Due to Ground Rupture

In this section, the influence of the existence of a pile on the responses of the ground and pile under the same fault dislocation condition is investigated. In this parametric study, we consider a square reinforced concrete pile with a size and length of 1.5 and 26 m, respectively, which is 25 m embedded into the ground. The elasticity modulus and Poisson's ratio of the pile are 17.3 GPa and 0.3, respectively. The coefficient of friction of the pile-soil interface is set to 0.5 following NAVRAC DM 7.2 (1982). To understand the foundation's response under reverse faulting, the position of the pile with respect to the fault tip is varied. As detailed in Fig. 10, three relative distances, x_I = 5 m, x_{II} = 10 m, and x_{III} = 15 m, are considered.

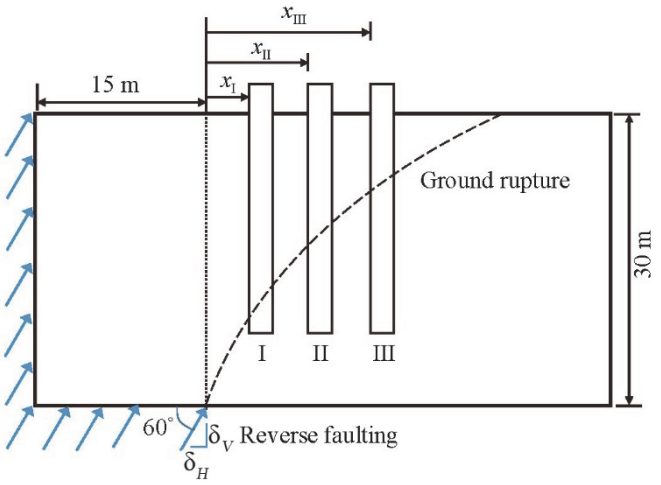

Fig. 10 Schematic of the position of single piles with respect to the fault tip

3.2.1 x_I = 5 m

Figure 11 presents the analysis results for x_I = 5 m. Figures 11(a) to 11(d) shows a comparison of the displacement and plastic shear strain fields at fault offsets of δ_V/H = 2% and 10%. At the smaller fault offset (Figs. 11(a) and 11(b) for δ_V/H = 2%), the main plastic shear strain (ground rupture) zone is limited in size and concentrated around the area between the fault tip and pile tip; the ground and pile displacements are small. At the larger fault offset (Figs. 11(c) and 11(d) for δ_V/H = 10%), the displacement and plastic shear strain fields are similar to those observed under the free-field condition (Fig. 8); the main area that is influenced is that near the pile tip. The pile is rotated and displaced together with the ground because its base is in the rupture band. Figure 11(e) shows a comparison of the ground displacement profile next to the pile with that under the free-field condition. The ground displacements above the rupture zone are similar, whereas those below the rupture zone exhibit a greater difference, implying that the influence of the rupture on the pile. Besides, the ground displacement profile is smoother because of the pile. The pile displacement, moment, and axial force increase with increasing fault offset, as illustrated in Figs. 11(f) to 11(h). For this case, the ground rupture zone is at a depth of approximately 18-25 m, and a clear turning point thus exists in the pile displacement curve (for depth of approximately 18 m). The maximum positive and negative moments occur at depths of approximately 17-20 and 8-10 m, respectively. The positions of the rupture zone and maximum positive moment move upward with increasing fault offset. The pile axial force is under tension; the depth of the maximum axial force decreases with increasing fault offset.

3.2.2 x_{II} = 10 m

Figure 12 presents the analysis results for x_{II} = 10 m. Figures 12(a) to 12(d) show a comparison of the displacement and plastic shear strain fields at fault offsets of δ_V/H = 2% and 10%. Similar to the case of x_I = 5 m, at the same smaller fault offset (δ_V/H = 2%), the pile and ground displacements are small. However, at the larger fault offset (δ_V/H = 10%), the ground displacement and plastic shear zones are strongly influenced and the pile seems to sustain substantial bending. Figure 12(e) shows a comparison of the ground displacement profile next to the pile with that under the free-field condition. At the smaller fault offset, the ground displacements are similar, whereas at the larger fault offset, the ground displacements are considerably different. The ground displacement profile under the free-field condition exhibits a large and abrupt change at a depth of about 11-13 m, whereas for ground with a pile, the displacement profile (solid line) is smooth and shows a significant displacement change near a depth of 9-10 m, implying that the development of ground rupture is limited and its path moves upward (Fig. 12(d) *vs.* Fig. 8(b)). The pile displacement, moment, and axial force profiles with increasing fault offset are shown in Figs. 12(f) to 12(h). Notably, the pile displacement has a clearly different shape from that for x_I = 5 m at larger fault offsets. When δ_V/H < 6%, the pile displaces in an approximately linear shape; when $\delta_V/H \geq$ 6%, the pile significantly bends to the right. For this case, as the ground rupture zone is at a depth of approximately 4-12 m, a large portion of the pile is in the footwall. Therefore, the displacement of the upper portion of the pile is considerably affected, whereas the lower portion of the pile displaces less. The moment profiles change with increasing fault offset. The moment profiles at small fault offsets are similar to those for x_I = 5 m. At large offsets, the moment profiles become different and only exhibit negative moments; the maximum moment occurs at a depth of approximately 10 m. Regarding the axial force profiles, the entire pile is under tension and the depth of the maximum axial force decreases with increasing fault offset.

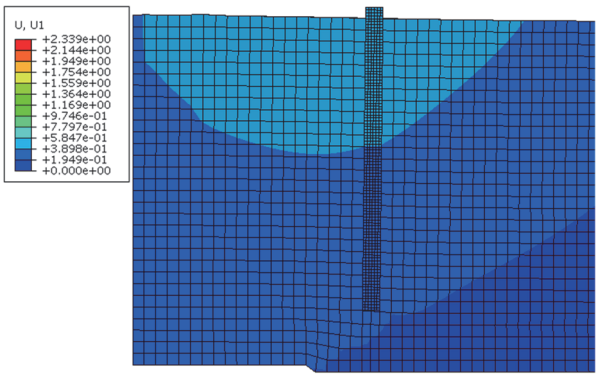

(a) Displacement field (δ_V/H = 2%)

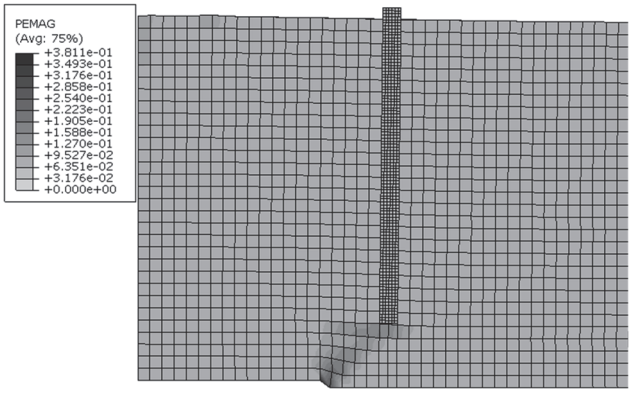

(b) Plastic shear strain field (δ_V/H = 2%)

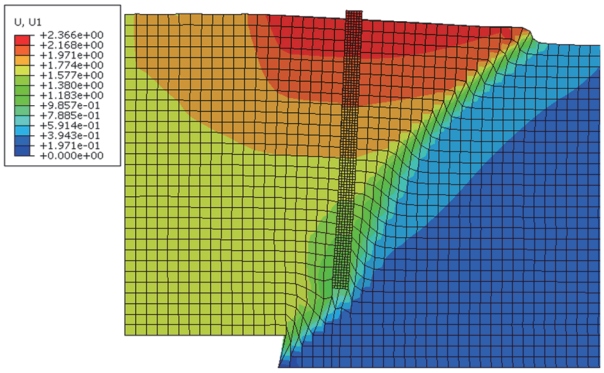

(c) Displacement field (δ_V/H = 10%)

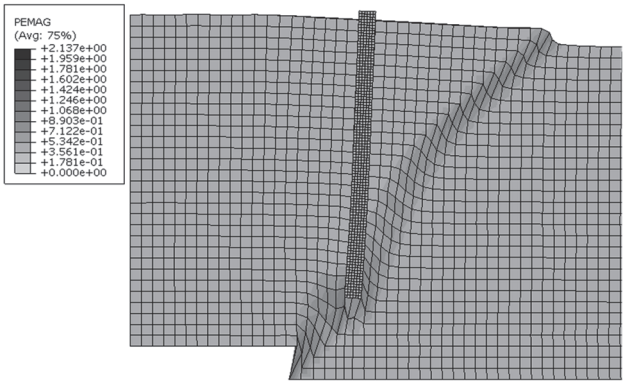

(d) Plastic shear strain field (δ_V/H = 10%)

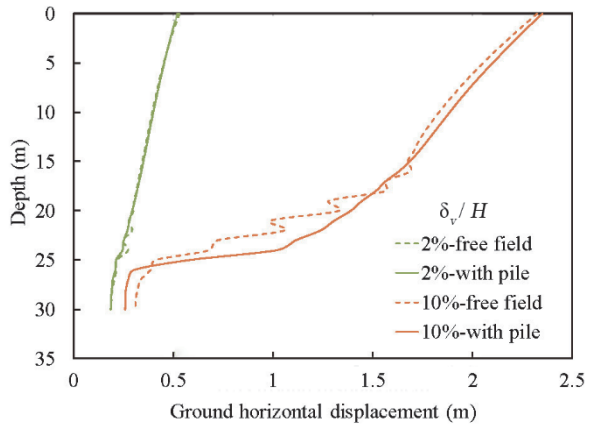

(e) Ground displacement

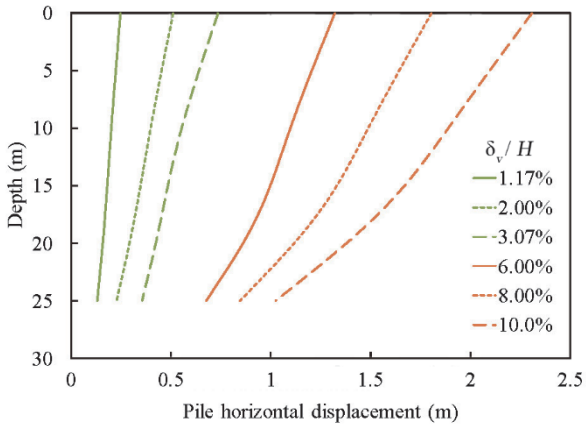

(f) Pile displacement

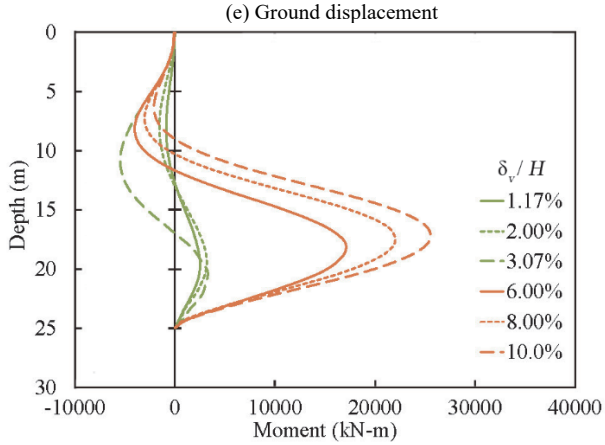

(g) Pile moment

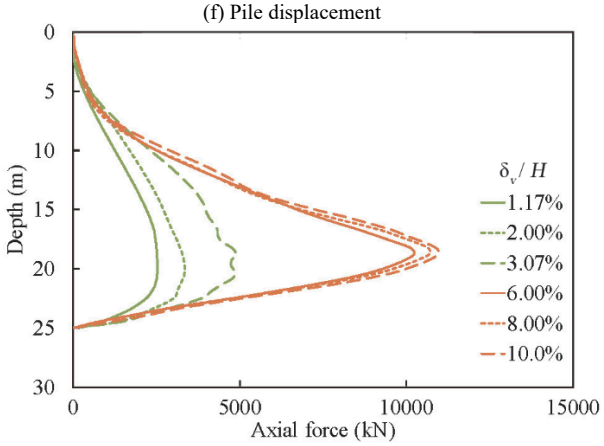

(h) Pile axial force

Fig. 11 Ground and pile responses under reverse faulting (x_1 = 5 m)

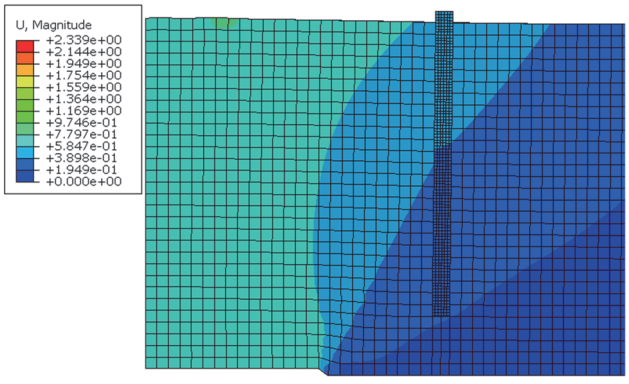

(a) Displacement field (δ_t/H = 2%)

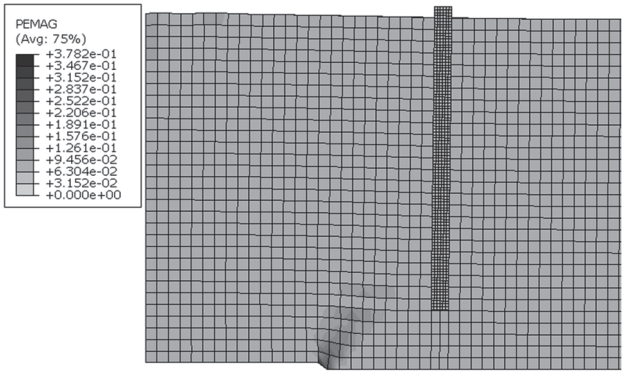

(b) Plastic shear strain field (δ_t/H = 2%)

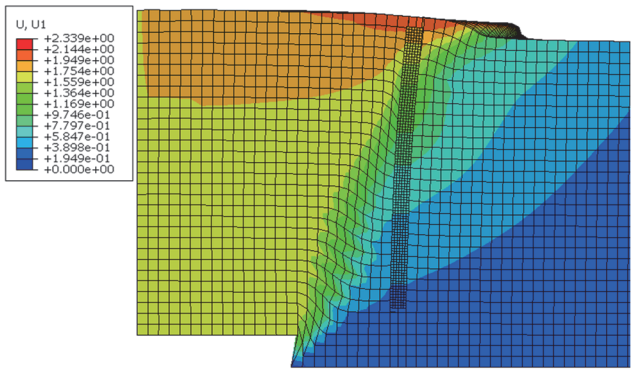

(c) Displacement field (δ_t/H = 10%)

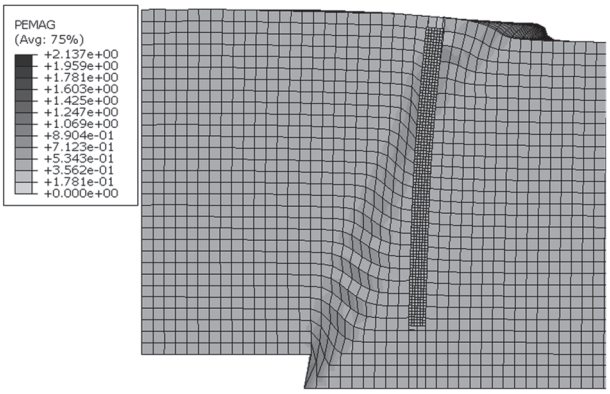

(d) Plastic shear strain field (δ_t/H = 10%)

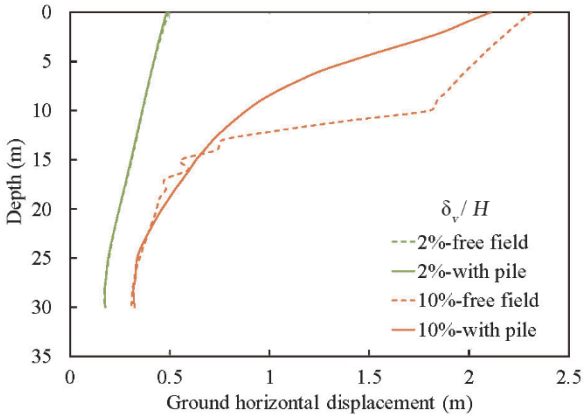

(e) Ground displacement

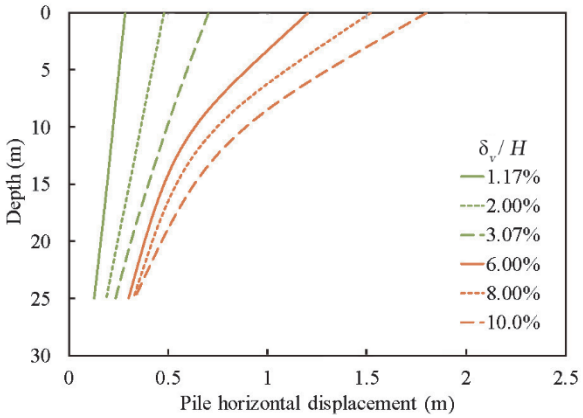

(f) Pile displacement

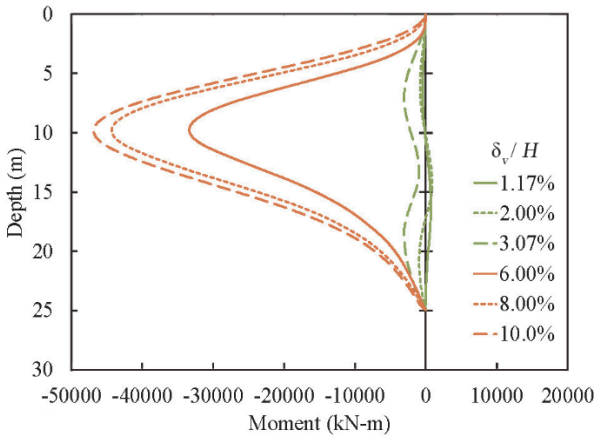

(g) Pile moment

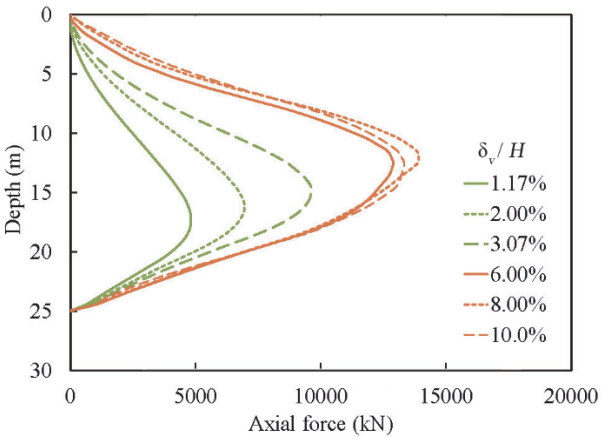

(h) Pile axial force

Fig. 12 Ground and pile responses under reverse faulting (x_{II} = 10 m)

3.2.3 x_{III} = 15 m

Figure 13 presents the analysis results for x_{III} = 15 m. Figures 13(a) to 13(d) shows a comparison of the displacement and plastic shear strain fields at fault offsets of δ_v/H = 2% and 10%. Because of the large relative distance between the pile and fault tip, the pile is less influenced by the fault than in the previous two cases. Figure 13(e) shows a comparison of the ground displacement profile next to the pile with that under the free-field condition. The existence of the pile clearly leads to a different ground rupture path; the rupture zone is moved upward. The pile displacement, moment, and axial force increase with increasing fault offset, as shown in Figs. 13(f) to 13(h). The ground rupture zone is at a depth of approximately 2 m. The trend in the pile displacement with changing fault offset is similar to that for x_{II} = 10 m. Notably, the

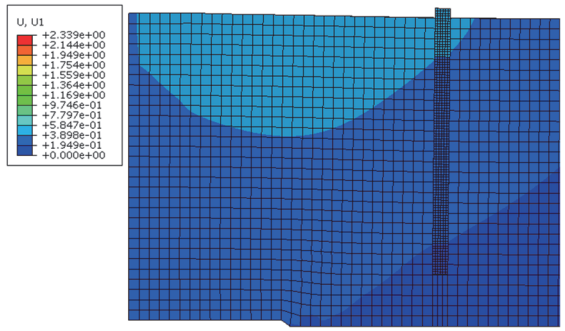

(a) Displacement field (δ_v/H = 2%)

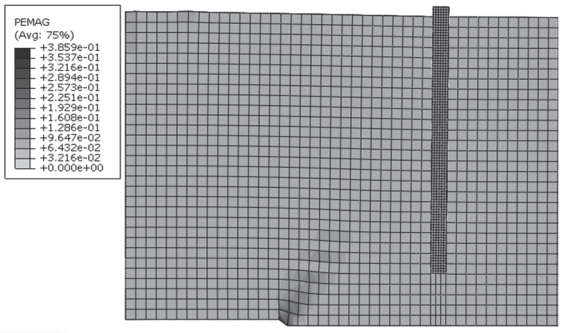

(b) Plastic shear strain field (δ_v/H = 2%)

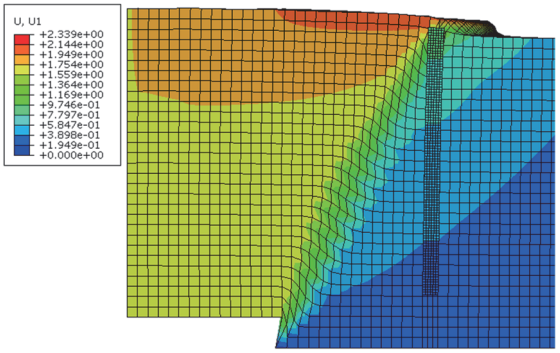

(c) Displacement field (δ_v/H = 10%)

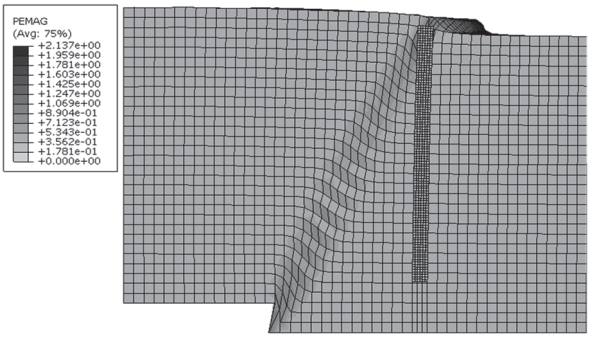

(d) Plastic shear strain field (δ_v/H = 10%)

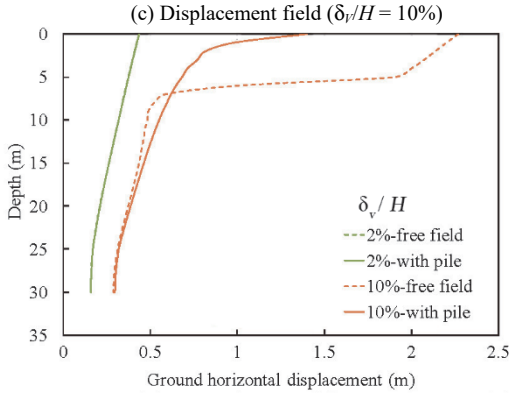

(e) Ground displacement

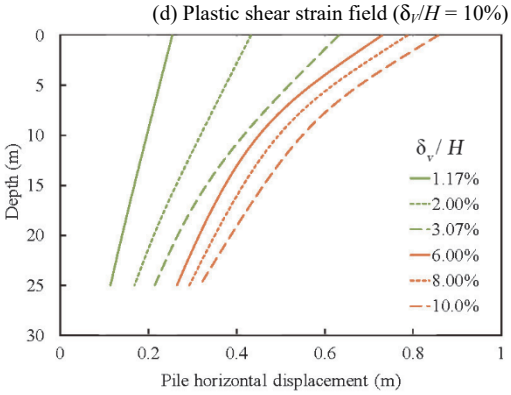

(f) Pile displacement

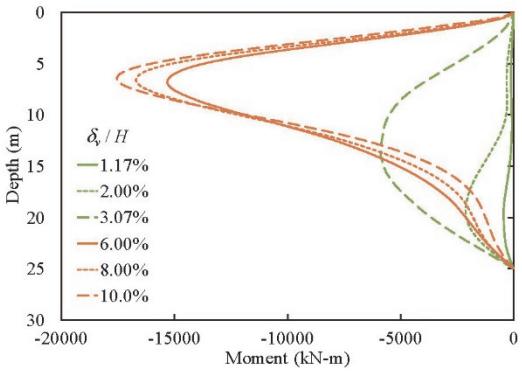

(g) Pile moment

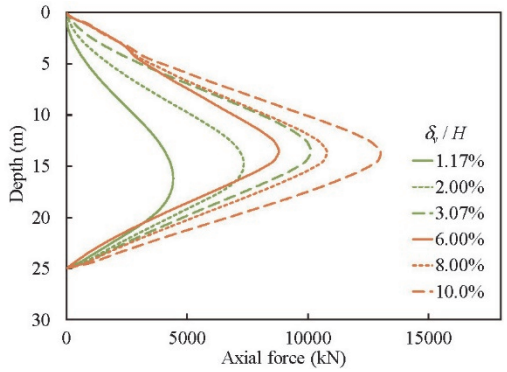

(h) Pile axial force

Fig. 13 Ground and pile responses under reverse faulting (x_{III} = 15 m)

pile moment is negative at all depths for the various fault offsets; the position of the maximum moment moves upward with increasing fault offset. The depth of the maximum axial force is similar for various fault offsets.

4. RESPONSE MECHANISMS OF PILE UNDER REVERSE FAULTING

The parametric analyses detailed in Section 3 reveal that when the foundation exists, it influences the path of development of ground ruptures, resulting in different foundation responses at various positions. This section identifies several fundamental response mechanisms by considering the detailed pile-soil interaction in reverse faulting and explains the evolution of the response mechanisms.

4.1 Classification of Pile Response Mechanisms

When the pile is subjected to reverse faulting, the soil is mainly in the passive state. The pile response is dependent on whether the ground rupture reaches the pile. Regarding before the ground rupture reaches the pile, the mechanisms underlying the pile response can be divided into three types on the basis of the position of the main strain zone acting on the pile; regarding after the ground rupture zone reaches the pile, the mechanisms underlying the pile response can be divided into two types in accordance with the position of the rupture on the pile. These five mechanisms are described in the following.

4.1.1 Mechanism A

When the fault offset is small, the ground rupture zone does not reach the pile and the stress is concentrated near the fault tip and spreads to the pile through the soil. If the main strain zone caused by faulting acts at a depth deeper than two-thirds of the embedded depth of the pile, the response mechanism of the pile is classified as Mechanism A. In this mechanism, illustrated in Fig. 14, ground deformation imposes loading at the lower part of the pile, and the pile displaces into an inclined S shape, consisting of rigid body rotation and an S-shape deflection. The soil reactions of both sides of the pile with respect to the at-rest earth pressure are negative (a negative value represents the soil pressure larger than the at-rest earth pressure), implying that the soil is in a passive state. Application of ground deformation at the lower part of the pile causes net soil reactions of the bottom soil to the right; therefore, the pile near the base (*i.e.*, lower half of the pile) sustains positive moments. Because the pile inclines to the right, the soil reactions on the right-hand side of the upper half of the pile are larger than those on the left-hand side of the pile, which causes negative moments in the pile.

4.1.2 Mechanism B

When the main strain zone caused by faulting acts at a depth of around one-third to two-thirds of the embedded depth of the pile before the ground rupture reaches the pile, the response mechanism of the pile is classified as Mechanism B. In this mechanism, displayed in Fig. 15, ground deformation imposes loading at the middle part of the pile, and in addition to rigid body rotation, the pile deflects into an approximately double sine shape. As mentioned in Mechanism A, a positive moment zone occurs around the location of the main strain zone (in the middle of the pile), and the displacements of the upper and lower parts of the pile are limited by the soil, which causes net soil reactions around these areas toward the left and results in negative moments in the pile.

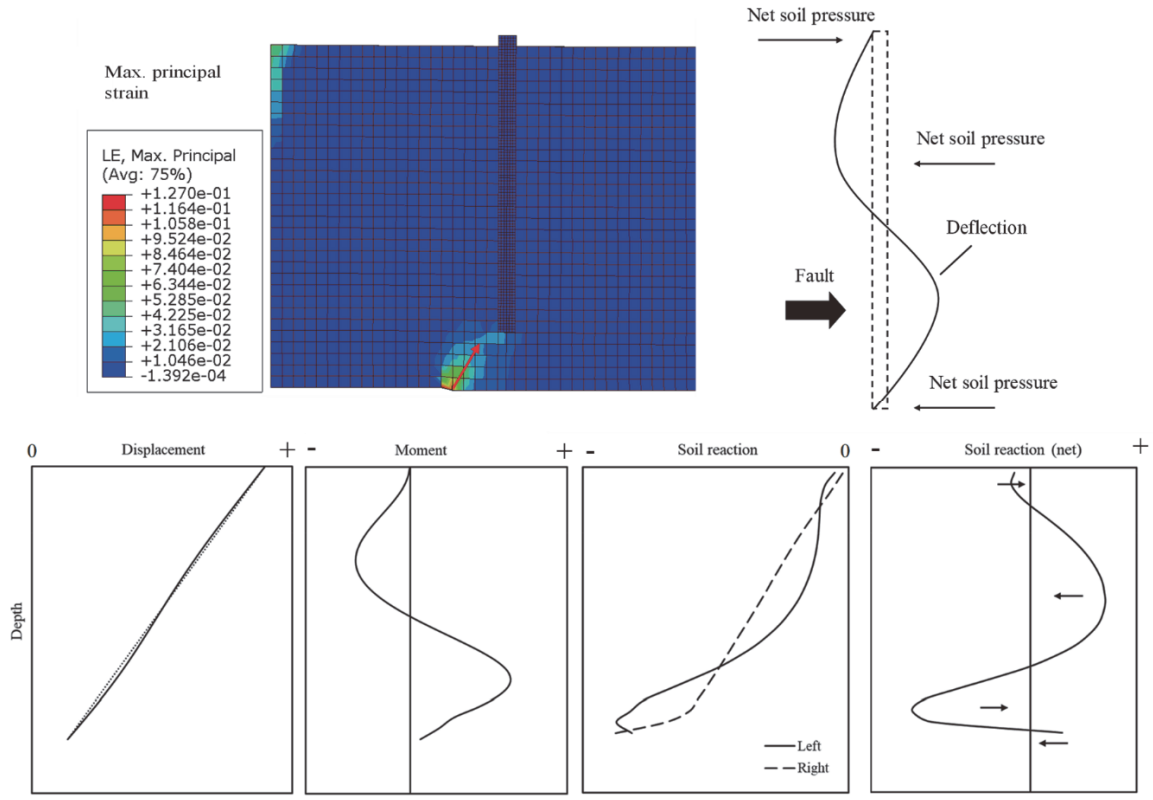

Fig. 14 Mechanism A

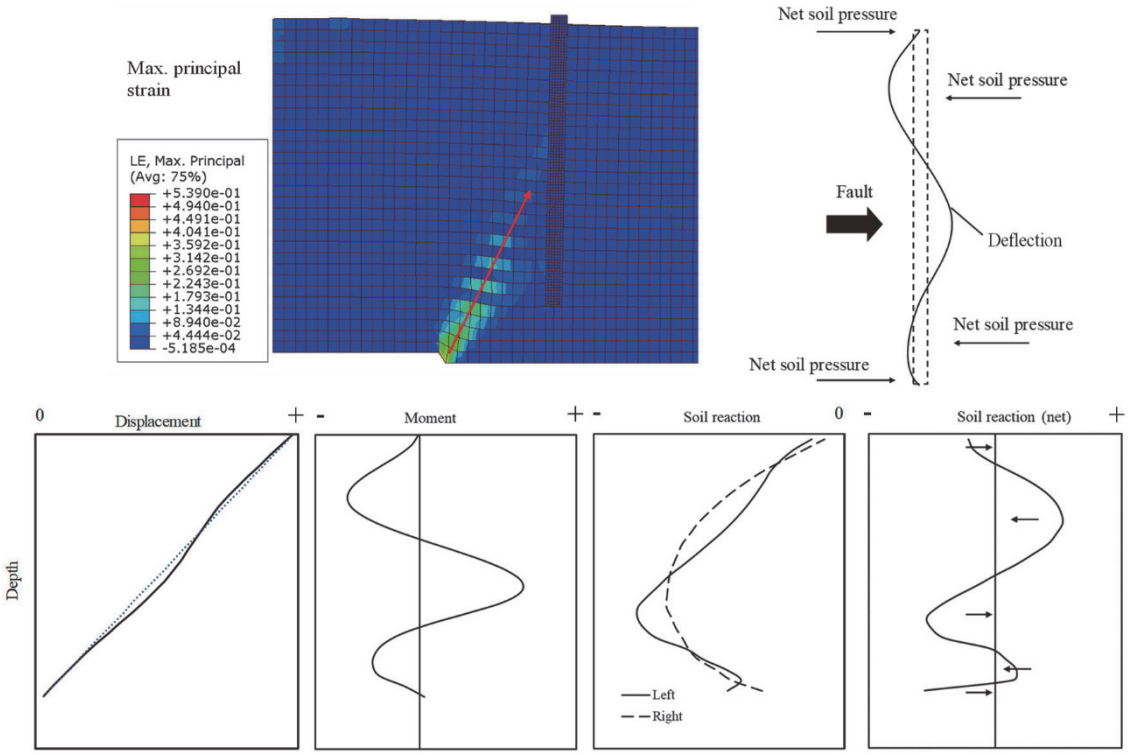

Fig. 15 Mechanism B

4.1.3 Mechanism C

When the main strain zone caused by faulting acts at a depth above one-third of the embedded depth of the pile before the ground rupture zone reaches the pile, the response mechanism of the pile is classified as Mechanism C. In this mechanism, illustrated in Fig. 16, ground deformation imposes loading at the upper part of the pile, and the pile concaves leftward. At the upper portion of the pile, the soil reactions on the left side of pile are larger than those on the right side (the net soil reactions are toward the right); for the lower part of the pile, because of the pile's deflection, most soil reactions on the right side of the pile are larger than those on the left side (the net soil reactions are toward the left). Therefore, the entire pile sustains negative moments.

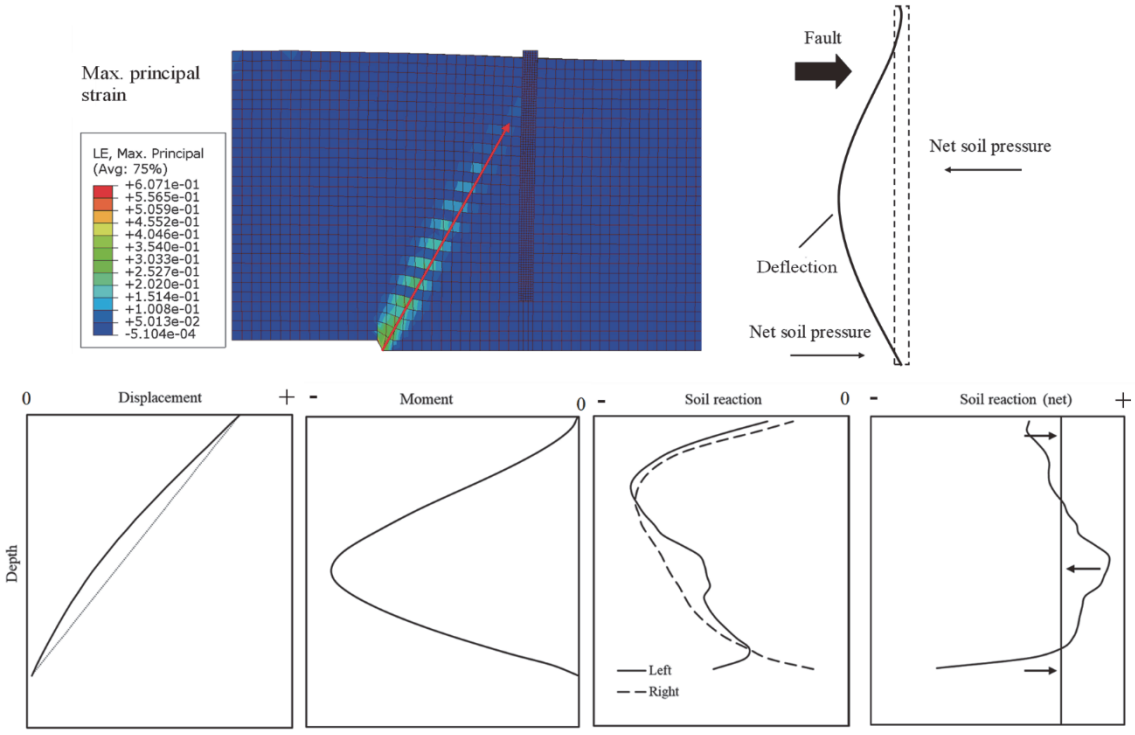

Fig. 16 Mechanism C

4.1.4 Mechanism D

As the fault offset continues to increase, the ground rupture zone gradually develops. If the ground rupture zone is located near the base of the pile—most of the pile is located on the hanging wall—the response mechanism of the pile is classified as Mechanism D. In this mechanism, illustrated in Fig. 17, a ground rupture occurs and is concentrated in the area near the pile base. Compared with the situation before the rupture reaches the pile, the pile is subject to large ground movement near the rupture because the action is concentrated at the rupture. This mechanism is similar to Mechanism A. When the hanging wall moves, the pile displaces with the ground and exhibits rotation at the tip. The ground rupture imposes large soil reactions on the pile, causing a large shear around the rupture zone. The position of the maximum moment varies depending on the position of the ground rupture zone. This response mechanism can also be observed in the verification case in Section 2.3, which is SP2 in Case RP80 reported in Yao and Takemura (2020).

4.1.5 Mechanism E

If the ground rupture zone is located at the upper half of the pile, the response mechanism of the pile is classified Mechanism E. In this mechanism, illustrated in Fig. 18, ground rupture occurs at the upper part of the pile. Because the pile is embedded in the footwall and the ground rupture acts on the upper half of the pile, the entire pile deflects to the right. The action is mainly concentrated at the rupture zone; at this time, the pile response is similar to that of the pile subjected to pile-head loading; it exhibits negative moments, and the position of the maximum moment is in the footwall and is affected by the embedded depth of the pile in the footwall. This response mechanism can also be observed in SP3 in Case RP80 reported in Yao and Takemura (2020), in which the distance between SP3 and the rupture is large compared with SP2.

4.2 Evolution of Pile Response Mechanisms

Figures 11(f) and 11(g) present the displacement and moment distributions of the pile at x_{I} = 5 m, respectively, with increasing fault offset. Under a small fault offset, the ground rupture zone does not reach the pile. Because the pile is close to the fault tip, the main strain zone caused by the fault acts at a position deeper than two-thirds of the embedded length of the pile. Under this condition, the pile response follows Mechanism A, as indicated by the green lines in the figure. As the fault offset increases, after the rupture zone reaches the pile near the pile tip, the pile is displaced with the hanging wall, and the pile response follows Mechanism D, as indicated by the orange lines in the figure.

Figures 12(f) and 12(g) present the displacement and moment distributions of the pile at x_{II} = 10 m, respectively, with increasing fault offset. Under a small fault offset, the ground rupture zone does not fully form. The main strain zone caused by faulting first acts on a position deeper than two-thirds of the embedded depth of the pile. The pile response in this state follows Mechanism A, as indicated by the green line at the offset of 1.17% in the figure. As the fault offset increases, the main strain zone shifts up to the middle of the pile, and the pile response follows Mechanism B, as indicated by the green line at the offset of 2% in the figure. The upper and lower parts of the pile are subjected to the net soil reactions to the left. As the fault offset keeps increasing until the rupture zone reaches the pile, the rupture zone is at the upper half of the foundation, and the pile response follows Mechanism E, as indicated by the orange lines in the figure. At this time, the pile sustains a large moment and undergoes substantial flexural deformations; the maximum moment occurs near the ground rupture zone.

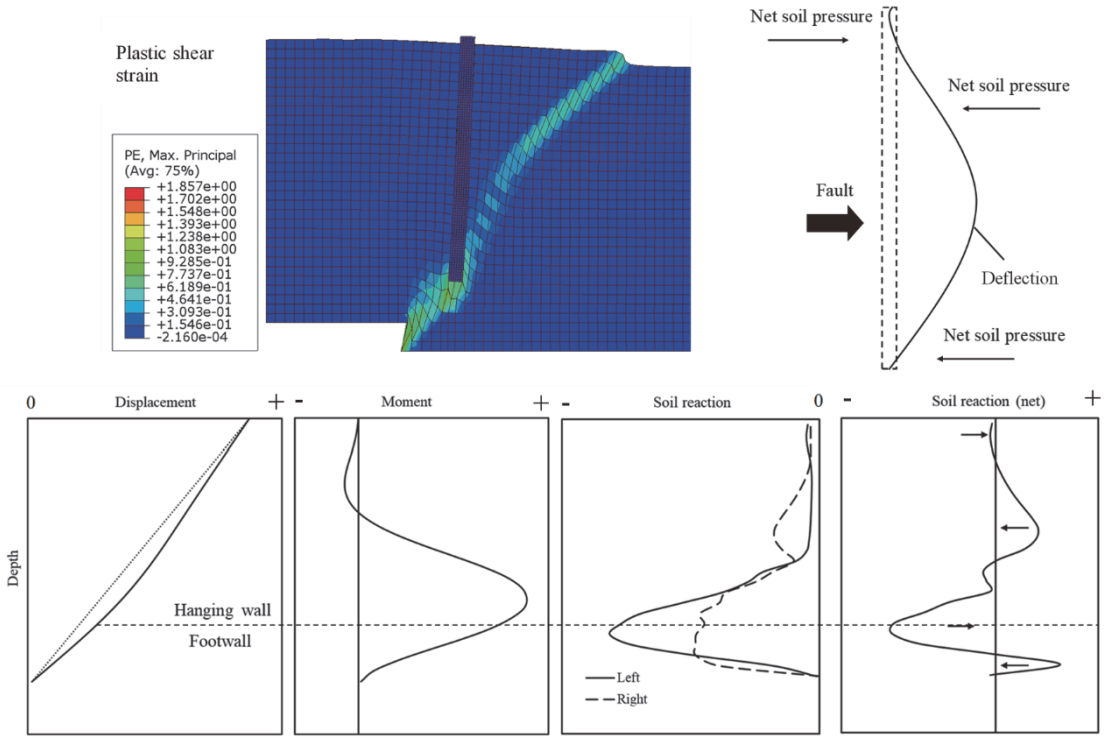

Fig. 17 Mechanism D

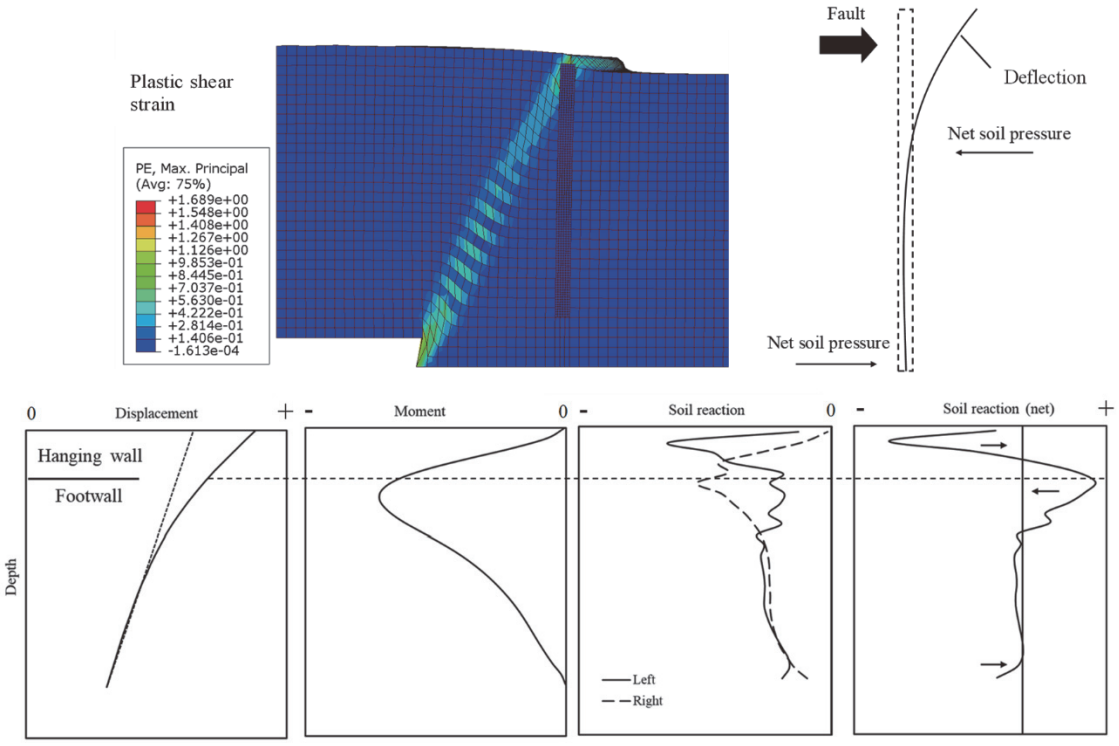

Fig. 18 Mechanism E

Figures 13(f) and 13(g) present the displacement and moment distributions of the pile at x_{III} = 15 m, respectively, with increasing fault offset. Under a small fault offset, the ground rupture zone does not reach the pile. Because the pile is far from the fault, the main strain zone caused by faulting acts at a depth less than one-third of the embedded depth of the pile. The pile response follows Mechanism C, as indicated by the green lines in the figure. As the fault offset increases, the position of the action moves upward; therefore, the position of the maximum moment also moves upward. The fault offset continues to increase until the ground rupture zone reaches the pile, and the ground rupture zone is then at the upper half of the pile, and the pile response follows Mechanism E, as indicated by the orange lines in the figure.

5. CONCLUSIONS

In this study, three-dimensional finite element analyses were performed to investigate the mechanisms underlying the responses of a single pile under reverse faulting. The pile and soil were modeled using solid elements. The soil model comprised the porous elasticity model combined with the Drucker-Prager/Cap model. The numerical model was validated by simulating a centrifuge test reported in the literature. Parametric analyses and comparisons of the displacement and plastic shear strain fields under the free-field condition and for ground containing a pile revealed the existence of the pile changed the ground rupture path from that under the free-field condition. The amount of fault offset and the relative distance between the pile and fault tip affected the pile response mechanism. On the basis of the position of the main strain area or the ground rupture zone caused by faulting on the pile, three and two mechanisms are identified for consideration of before and after the ground rupture zone reaches the pile, respectively.

The present study assumes an elastic pile. Piles may yield under the action of reverse faulting. Further studies can be performed to investigate the influence of pile yielding.

FUNDING

This work is funded by the Ministry of Science and Technology, Taiwan (Grant no. MOST 108-2628-E-002-004-MY3) and the National Taiwan University, Taiwan (Grant no. NTU-CC-112L894505).

DATA AVAILABILITY

Some or all data, models, or code that support the findings of this study are available from the corresponding author upon reasonable request.

CONFLICT OF INTEREST STATEMENT

The authors declare that they have no known conflict of interests or personal relationships that could have appeared to influence the work reported in this paper.

REFERENCES

ABAQUS (2012). *ABAQUS/CAE 6.12 User's Manual*. Online Documentation Help: Dassault Systèmes.

Anastasopoulos, I. and Gazetas, G. (2007). "Foundation-structure systems over a rupturing normal fault: Part I. Observations after the Kocaeli 1999 earthquake." *Bulletin of Earthquake Engineering*, **5**(3), 253-275. https://doi.org/10.1007/s10518-007-9029-2

Anastasopoulos, I., Gazetas, G., Bransby, M.F., Davies, M.C.R.,

and El Nahas, A. (2007). "Fault rupture propagating through sand: finite element analysis and validation through centrifuge experiments." *Journal of Geotechnical and Geoenvironmental Engineering*, ASCE, **133**(8), 943-958. https://doi.org/10.1061/(ASCE)1090-0241(2007)133:8(943)

Anastasopoulos, I., Gazetas, G., Drosos V., Georgarakos, T., and Kourkoulis, R. (2008a). "Design of bridges against large tectonic deformation." *Earthquake Engineering and Engineering Vibration*, **7**(4), 345-368. https://doi.org/10.1007/s11803-008-1001-x

Anastasopoulos, I., Callerio, A., Bransby, M.F., Davies, M.C.R., El Nahas, A., Faccioli, E., Gazetas, G., Masella, A., Paolucci, R., Pecker, A., and Rossignol, E. (2008b). "Numerical analyses of fault-foundation interaction." *Bulletin of Earthquake Engineering*, **6**, 645-675. https://doi.org/10.1007/s10518-008-9078-1

Bransby, M.F., Davies, M.C.R., EI Nahas, A., and Nagaoka, S. (2008). "Centrifuge modelling of reverse fault-foundation interaction." *Bulletin of Earthquake Engineering*, **6**, 607-628. https://doi.org/10.1007/s10518-008-9080-7

Cai, Q.P. and Ng, C.W.W. (2016). "Centrifuge modeling of pile-sand interaction induced by normal faulting." *Journal of Geotechnical and Geoenvironmental Engineering*, ASCE, **142**(10), 04016046. https://doi.org/10.1061/(ASCE)GT.1943-5606.0001500

Chen, C.H., Chou, H.S., Yang, C.Y., Shieh, B.J., and Kao, Y.H. (2003). "Chelungpu fault inflicted damages of pile foundations on FWY Route 3 and fault zoning regulations in Taiwan." *Proceedings of the 2nd Workshop on Seismic Fault-Induced Failures, Possible Remedial Measures for Civil Infrastructures*, edited by K. Konagai, M. Hori, and K. Meguro, 1-20. Tokyo: JSCE.

Faccioli, E., Anastasopoulos, I., Gazetas, G., Callerio, A., and Paolucci, R. (2008). "Fault rupture-foundation interaction: Selected case histories." *Bulletin of Earthquake Engineering*, **6**, 557-583. https://doi.org/10.1007/s10518-008-9089-y

Chiou, J.S. and Wei, W.T. (2021). "Numerical investigation of pile-head load effects on the negative skin friction development of a single pile in consolidating ground." *Acta Geotechnica*, **16**(6), 1867-1878. https://doi.org/10.1007/s11440-020-01134-0

Chiou, J.S. and You, J.Q. (2020). "Three-dimensional finite element analysis of laterally loaded bridge caisson foundations in gravelly soil." *Acta Geotechnica*, **15**(11), 3151-3166. https://doi.org/10.1007/s11440-020-00979-9

Fadaee, M., Hashemi, K., Farzaneganpour, F., Anastasopoulos, I., and Gazetas, G. (2020). "3-storey building subjected to reverse faulting: Analysis and experiments." *Soil Dynamics and Earthquake Engineering*, **138**, 106297. https://doi.org/10.1016/j.soildyn.2020.106297

Naeij, M., Soroush, A., and Javanmardi, Y. (2019). "Numerical investigation of the effects of embedment on the reverse fault-foundation interaction." *Computers and Geotechnics*, **113**, 103098. https://doi.org/10.1016/j.compgeo.2019.103098

NAVFAC DM-7.2. (1982). *Foundations and Earth Structures*. Department of the Navy Facilities Engineering Command, Alexandria.

Oettle, N.K. and Bray, J.D. (2013). "Geotechnical mitigation strategies for earthquake surface fault rupture." *Journal of Geotechnical and Geoenvironmental Engineering*, ASCE, **139**(11), 1864-1874. https://doi.org/10.1061/(ASCE)GT.1943-5606.0000933

Rasouli, H. and Fatahi, B. (2019). "A novel cushioned piled raft foundation to protect buildings subjected to normal fault rupture." *Computers and Geotechnics*, **106**, 228-248. https://doi.org/10.1016/j.compgeo.2018.11.002

Yang, S. and Mavroeidis, G.P. (2018). "Bridge crossing fault rupture zones: A review." *Soil Dynamics and Earthquake Engineering*, **113**, 545-571. https://doi.org/10.1016/j.soildyn.2018.03.027

Yao, C. and Takemura, J. (2019). "Using laser displacement transducer scanning technique in centrifuge modeling of reverse fault-foundation interaction." *Soil Dynamics and Earthquake Engineering*, **121**(3), 219-232. https://doi.org/10.1016/j.soildyn.2019.03.018

Yao, C. and Takemura, J. (2020). "Centrifuge modeling of single piles in sand subjected to dip-slip faulting." *Journal of Geotechnical and Geoenvironmental Engineering*, ASCE, **146**(3), 04020001. https://doi.org/10.1061/(ASCE)GT.1943-5606.0002202